

# CURVILINEAR SHORECIRC

## Users Manual

A Curvilinear Version of Quasi-3D Nearshore Circulation Model

Fengyan Shi, Ib A. Svendsen, and James T. Kirby  
Center for Applied Coastal Research  
University of Delaware  
Newark, DE 19716 USA

## **Abstract**

The curvilinear version of the nearshore circulation model SHORECIRC is developed based on the quasi-3D nearshore circulation equations derived by Putrevu and Svendsen (1999). The Users Manual is comprised of a brief introduction to the theory, numerical methodology, and sample problems that demonstrate the capabilities of the Curvilinear SHORECIRC model.

In reading this manual, you will find it useful to have the SHORECIRC Manual and the Master Program Manual handy since the Curvilinear SHORECIRC model is heavily dependent on the Cartesian version of SHORECIRC for its theory and underlying architecture, and the CURVILINEAR SHORECIRC is a subroutine linked by the Master Program in the Nearshore Community Model. In this manual, we only discuss the differences between the Cartesian version and Curvilinear version of the SHORECIRC model in numerical methods and model setup.

# Contents

<b>1</b>	<b>Introduction</b>	<b>5</b>
<b>2</b>	<b>SHORECIRC Equations in Curvilinear Coordinates</b>	<b>7</b>
2.1	Coordinate transformation . . . . .	7
2.2	Depth-integrated, short-wave-averaged equations . . . . .	8
2.3	Calculation of vertical current profiles . . . . .	9
2.4	Boundary conditions . . . . .	10
2.4.1	Wall boundary . . . . .	10
2.4.2	Flux boundary . . . . .	10
2.4.3	Surface elevation boundary . . . . .	10
2.4.4	Periodic boundary . . . . .	11
2.4.5	Moving boundary . . . . .	11
<b>3</b>	<b>Numerical Scheme</b>	<b>11</b>
3.1	Staggered grid . . . . .	11
3.2	High-order numerical scheme . . . . .	11
3.3	Second-order semi-implicit scheme . . . . .	12
<b>4</b>	<b>Model Structure and Program</b>	<b>13</b>
4.1	Flowchart . . . . .	13
4.2	Subroutines . . . . .	14
4.3	Model input . . . . .	22
4.4	Model output . . . . .	25
4.5	Passing variables in model coupling . . . . .	26
<b>5</b>	<b>Curvilinear Grid Generation</b>	<b>28</b>
<b>6</b>	<b>Test Examples</b>	<b>28</b>
6.1	Longshore current simulation in an obliquely quadrilateral domain . . . . .	28
6.1.1	General model description . . . . .	29
6.1.2	Input files . . . . .	29
6.1.3	Results . . . . .	37
<b>7</b>	<b>References</b>	<b>42</b>

## List of Figures

1	Staggered grid in $\xi_1 - \xi_2$ plane ( $\times$ — $\bar{\zeta}$ point, $\bigcirc$ — $\tilde{V}^1$ and $\square$ — $\tilde{V}^2$ ). . . . .	12
2	Flowchart of CURVILINEAR SHORECIRC . . . . .	15
3	Plan view of the LSTF. . . . .	30
4	Computational grid. . . . .	37
5	Depth-averaged current velocity field. . . . .	38
6	Longshore current comparisons at the measurement transects (circles: measurement, solid lines: numerical results). . . . .	39
7	Mean water level comparisons at the measurement transects (circles: measurement, solid lines: numerical results). . . . .	40
8	Comparison of the vertical profile of cross-shore current at Y27 (circles: measurement, solid lines: numerical results). . . . .	41

# 1 Introduction

The performance of a numerical model for wave-induced nearshore circulation is important for predicting sediment and pollutant transport in coastal regions. The model performance mainly depends on the understanding of nearshore phenomena as well as numerical techniques used in the model. Over the last decades, significant progress has been made in our understanding of wave-generated phenomena such as wave set-up, wave breaking, undertow, cross-shore and longshore currents and their stability, turbulence and mixing, and the generation of long-wave phenomena. Based on this understanding, a variety of numerical models have been developed and used for modeling of nearshore phenomena.

Recently, the three-dimensional dispersion of momentum in wave-induced nearshore currents was discussed by Svendsen and Putrevu (1994). They found that the vertical nonuniformity of the currents leads to a mixing-like term in the depth-integrated along-shore momentum equation, which is analogous to the shear-dispersion mechanism found by Taylor (1953, 1954). The lateral mixing caused by the shear-dispersion mechanism is an order of magnitude larger than the turbulent lateral mixing and is thus considered to be a major contributor to the total lateral mixing in the nearshore region. Smith (1997) also presented a rather general derivation of the shear dispersion mechanism for the case with no short-wave-induced volume flux. Putrevu and Svendsen (1999, PS99 hereafter) extended the results of Svendsen and Putrevu (1994) to the general case of unsteady circulations induced by wave breaking over an arbitrary bottom topography. For a zero wave-induced volume flux, the newly derived equations are similar to those of Smith. A quasi-3D numerical model named SHORECIRC (Svendsen, et al., 2000) has been developed based on the nearshore circulation equations. It is a 2D horizontal model which incorporates the effect of the vertical structure of horizontal flows. A semi-analytical solution is used for the 3D current profiles in combination with a numerical solution for the depth-integrated 2D horizontal equations. Several applications of the model have been carried out in studies of various nearshore phenomena, such as surf-beat (Van Dongeren *et al.*, 1995), longshore currents (Sancho *et al.*, 1995), infragravity waves (Van Dongeren et al., 1996, 1998, 2000), shear waves (Sancho and Svendsen, 1998) and rip currents (Haas *et al.*, 1998, Svendsen and Haas, 1999) and the model has been compared to data from the DELILAH field experiment (Svendsen *et al.*, 1997).

The SHORECIRC model was developed in rectangular Cartesian coordinates and was only used in rectangular domains, thus limiting the applicability of the model to less complicated coastal environments. First, a rectangular grid is not able to fit complicated shoreline boundaries very well. Second, complicated geometries, such as harbors and tidal inlets,

make the uniform-resolution model very expensive when a fine grid is used. Therefore, the development of a curvilinear version of SHORECIRC is necessary for its use in irregular shaped domains.

There are numerous examples of curvilinear grid methods in the study of waves and currents. Usually structured grid methods with finite-difference discretizations, or unstructured grid methods with a finite-element or finite-volume approach are used in model developments. Unstructured grids are more flexible than structured grids to fit complicated boundaries and are able to deal with very complex geometries. However, the finite-difference methods with structured curvilinear grids are much simpler to program than finite-element or finite-volume methods and thus are widely used in fluid dynamic fields. For example, Blumberg and Mellor (1987) developed a 3D coastal ocean circulation model (POM) in orthogonal curvilinear coordinates. Non-orthogonal boundary-fitted grid models with generalized coordinate transformation were developed by many authors (e.g., Sheng, 1986; Shi and Sun, 1995; Shi *et al.*, 1997) for modeling coastal and estuarine processes.

For a generalized coordinate transformation, several advantages of using the contravariant technique have been recognized in the derivations of hyperbolic-type equations, as shown by Sheng (1986) and Shi and Sun (1995), among others. In generalized curvilinear coordinates, contravariant and covariant components are two kinds of vector components based on, respectively, a basis which is locally tangent to the curvilinear coordinate and a reciprocal basis which is locally normal to the curvilinear coordinate. The designation “contravariant” or “covariant” technique represents the choice of components which are adopted as primitive variables in the equations transformed from rectangular Cartesian coordinates. It has been found that both the contravariant technique and the covariant technique are able to simplify the transformed equations (see, for example, Warsi, 1998), in comparison to the Cartesian component method (see, for example, Häuser *et al.*, 1985, 1986; Raghunath *et al.*, 1987; Borthwick and Barber, 1992). The contravariant technique can simplify slip lateral boundary conditions compared to the covariant technique and is thus more conveniently used in hydrodynamic models with slip boundary conditions.

The present model, the curvilinear nearshore circulation model (Curvilinear SHORECIRC), is developed based on the quasi-3D circulation equations. A generalized coordinate transformation and the contravariant technique are used in the model. In numerics, the Curvilinear SHORECIRC provides two options respectively based on high-order explicit numerical schemes and second-order semi-implicit schemes. The high-order explicit schemes follow the Cartesian version of SHORECIRC (Svendsen *et al.*, 2000). A fourth-order Adams-Bashforth-Moulton predictor-corrector scheme is employed to perform the time integration and a fourth-order scheme using standard five-point finite differencing is

used in the first-order derivative terms, while a second-order scheme is used for the higher order derivatives and coordinate metrics for spatial discretizations. The second-order semi-implicit numerical schemes are developed based on a splitting method in which the gravity wave mode and vorticity wave mode are solved separately. The semi-implicit numerical schemes are basically CFL-free schemes and thus are more efficient for long-term simulations. Unlike the spatial discretization in the Cartesian version, we use a staggered grid system in the transformed image domain. Various point types are defined in the model code to recognize different boundary conditions, which allows the model to be used in complicated domains such as harbors and tidal inlets. The point-type specification can be done by either using the grid generation program **CoastGrid** or specifying negative water depths at land points. The Curvilinear SHORECIRC also has a capability of water flooding calculations.

A test example is provided in the Users Manual. The test case shows the longshore current simulations for the longshore current experiment conducted at US Army Engineer Research and Development Center (Hamilton and Ebersole, 2001). A non-rectangular grid is employed to fit the oblique waveguides used in the physical experiment.

It is highly recommended that anyone wanting to apply the present model should first gain a familiarity with the SHORECIRC documentation in Svendsen et al (2002).

## 2 SHORECIRC Equations in Curvilinear Coordinates

### 2.1 Coordinate transformation

A coordinate transformation is introduced in the general form

$$\begin{cases} \xi_1 = \xi_1(x_1, x_2) \\ \xi_2 = \xi_2(x_1, x_2) \\ z = z \end{cases} \quad (1)$$

where  $(x_1, x_2, z)$  are spatial independent variables in rectangular Cartesian coordinates and  $(\xi_1, \xi_2, z)$  are new independent variables in the transformed image domain.  $z$  represents the vertical coordinate. Any vector  $\mathbf{v}$  can be written in Cartesian coordinates as

$$\mathbf{v} = v_1 \mathbf{i} + v_2 \mathbf{j} + v_3 \mathbf{k}. \quad (2)$$

where  $(\mathbf{i}, \mathbf{j}, \mathbf{k})$  are Cartesian basis vectors. In the generalized curvilinear coordinates, the coordinate basis is the combination of the generalized horizontal basis  $(\mathbf{a}_1, \mathbf{a}_2)$  and the vertical Cartesian base vector  $\mathbf{k}$  and is written as  $(\mathbf{a}_1, \mathbf{a}_2, \mathbf{k})$ . Using the new basis  $(\mathbf{a}_1, \mathbf{a}_2, \mathbf{k})$ , the vector  $\mathbf{v}$  can be described as

$$\mathbf{v} = v^\alpha \mathbf{a}_\alpha + v_3 \mathbf{k} \quad (\alpha = 1, 2). \quad (3)$$

where  $v^\alpha$  are contravariant horizontal components of the vector;  $v_3$  is the vertical Cartesian component of the vector.

The relationship between horizontal components in the Cartesian and contravariant components in the curvilinear coordinates may be written as

$$v^\alpha = \frac{\partial \xi_\alpha}{\partial x_\beta} v_\beta \quad (\alpha, \beta = 1, 2). \quad (4)$$

where  $v_\beta$  represents the Cartesian components.

Following the velocity splitting method in PS99, the contravariant components of instantaneous horizontal velocity can be written as

$$u^\alpha = u'^\alpha + u_w^\alpha + \tilde{V}^\alpha + V_1^\alpha \quad (5)$$

where  $u'^\alpha$ ,  $u_w^\alpha$ ,  $\tilde{V}^\alpha$ , and  $V_1^\alpha$  are, respectively, the turbulence component, the wave component, the component of depth-averaged and short-wave-averaged velocity, and the vertical variation of the short-wave-averaged velocity.

## 2.2 Depth-integrated, short-wave-averaged equations

The depth-integrated, short-wave-averaged continuity equation and momentum equation (PS99, (4) and (45)) in terms of contravariant components are given by

$$\frac{\partial \bar{\zeta}}{\partial t} + \frac{1}{\sqrt{g_0}} \frac{\partial}{\partial \xi_\alpha} (\sqrt{g_0} \tilde{V}^\alpha h) = 0 \quad (6)$$

$$\begin{aligned} \frac{\partial}{\partial t} (\tilde{V}^\alpha h) &+ \frac{1}{\sqrt{g_0}} \frac{\partial}{\partial \xi_\beta} \left[ \sqrt{g_0} (\tilde{V}^\alpha \tilde{V}^\beta h + A_{\alpha\beta\delta} \tilde{V}^\delta) \right] + (\tilde{V}^\gamma \tilde{V}^\beta h + A_{\gamma\beta\delta} \tilde{V}^\delta) \Gamma_{\gamma\beta}^\alpha \\ &+ \frac{1}{\rho \sqrt{g_0}} \frac{\partial}{\partial \xi_\beta} \left[ \sqrt{g_0} (S^{\alpha\beta} + \rho M_{\alpha\beta}) \right] + \frac{1}{\rho} (S^{\gamma\beta} + \rho M_{\gamma\beta}) \Gamma_{\gamma\beta}^\alpha \\ &+ gh g^{\beta\alpha} \frac{\partial \bar{\zeta}}{\partial \xi_\beta} + \frac{\tau_B^\alpha}{\rho} + \frac{1}{\sqrt{g_0}} \frac{\partial}{\partial \xi_\beta} \left\{ \sqrt{g_0} \left[ T^{\alpha\beta} - h (D_{\delta\beta} \tilde{V}_{,\delta}^\alpha + D_{\delta\alpha} \tilde{V}_{,\delta}^\beta) \right] \right\} \\ &+ \left[ T^{\gamma\beta} - h (D_{\delta\beta} \tilde{V}_{,\delta}^\gamma + D_{\delta\gamma} \tilde{V}_{,\delta}^\beta) \right] \Gamma_{\gamma\beta}^\alpha \\ &- \frac{1}{\sqrt{g_0}} \frac{\partial}{\partial \xi_\beta} \left[ \sqrt{g_0} (h B_{\alpha\beta} \tilde{V}_{,\delta}^\delta) \right] - (h B_{\gamma\beta} \tilde{V}_{,\delta}^\delta) \Gamma_{\gamma\beta}^\alpha = 0 \end{aligned} \quad (7)$$

where  $g_0$  is the determinant of the metric tensor  $g_{\alpha\beta}$ ,

$$g_0 = \begin{vmatrix} g_{11} & g_{12} \\ g_{21} & g_{22} \end{vmatrix} \quad (8)$$

in which

$$g_{\alpha\beta} = \frac{\partial x_\gamma}{\partial \xi_\alpha} \frac{\partial x_\gamma}{\partial \xi_\beta} \quad (9)$$

and  $\Gamma_{\gamma\beta}^\alpha$  is Christoffel symbol of the second kind. The tensors  $A, B, D$  and  $M$  have the same definitions as in PS99 except all the horizontal derivatives of  $V_1^{(0)}$  should be replaced by the corresponding covariant derivatives.

It is noticed that  $\tau_s^\alpha$  and  $\tau_B^\alpha$  are the contravariant components of the surface shear stress and the bottom shear stress, respectively.  $S^{\alpha\beta}$  and  $T^{\alpha\beta}$  are the contravariant components of the short-wave-induced radiation stress tensor and the depth-integrated Reynolds' stress tensor, respectively. the relationship between  $S^{\alpha\beta}$  and  $S_{\alpha\beta}$  can be easily obtained as:

$$S^{11} = \frac{1}{g_0} \left( S_{11} \left( \frac{\partial x_2}{\partial \xi_2} \right)^2 - 2S_{12} \frac{\partial x_2}{\partial \xi_2} \frac{\partial x_1}{\partial \xi_2} + S_{22} \left( \frac{\partial x_1}{\partial \xi_2} \right)^2 \right) \quad (10)$$

$$S^{12} = S^{21} = \frac{1}{g_0} \left( -S_{11} \frac{\partial x_2}{\partial \xi_1} \frac{\partial x_2}{\partial \xi_2} + S_{12} \left( \frac{\partial x_1}{\partial \xi_1} \frac{\partial x_2}{\partial \xi_2} + \frac{\partial x_2}{\partial \xi_1} \frac{\partial x_1}{\partial \xi_2} \right) - S_{22} \frac{\partial x_1}{\partial \xi_1} \frac{\partial x_1}{\partial \xi_2} \right) \quad (11)$$

$$S^{22} = \frac{1}{g_0} \left( S_{11} \left( \frac{\partial x_2}{\partial \xi_1} \right)^2 - 2S_{12} \frac{\partial x_1}{\partial \xi_1} \frac{\partial x_2}{\partial \xi_1} + S_{22} \left( \frac{\partial x_1}{\partial \xi_1} \right)^2 \right) \quad (12)$$

Usually  $S_{\alpha\beta}$  is computed from a wave model and  $S^{\alpha\beta}$  is then obtained using (10) - (12). Another way to get the term  $S_{,\beta}^{\alpha\beta}$  is to calculate the contravariant component of  $\text{div}S$  from its Cartesian components which is directly obtained from a wave model in Cartesian coordinates.

### 2.3 Calculation of vertical current profiles

For the calculation of vertical variation of time-averaged currents, we also use the non-dimensional analysis and perturbation method as in PS99 the perturbation expansion gives the type

$$V_1^\alpha = V_1^{\alpha(0)} + \delta V_1^{\alpha(1)} + \dots \quad (13)$$

where  $\delta$  ( $\sim 0.1$ ) represents the size of the short-wave-induced quantities;  $V_1^{\alpha(0)}$  and  $V_1^{\alpha(1)}$  represent zero- and first-order of the contravariant components. We only consider the first term on the right hand side of (13) in the present model. The governing equation for  $V_1^{\alpha(0)}$  is

$$\frac{\partial V_1^{\alpha(0)}}{\partial t} - \frac{\partial}{\partial z} \left( \nu_t \frac{\partial V_1^{\alpha(0)}}{\partial z} \right) = F^\alpha \quad (14)$$

where

$$F^\alpha = \frac{1}{\rho h} S_{,\beta}^{\alpha\beta} - f^\alpha + \frac{\tau_B^\alpha}{\rho h} \quad (15)$$

$V_1^{\alpha(0)}$  is given by

$$V_1^{\alpha(0)} = d_{1\alpha} \xi^2 + e_{1\alpha} \xi + f_{1\alpha} + f_{2\alpha} \quad (16)$$

where

$$\xi = z + h \quad (17)$$

in which  $h$  is the water depth from the mean water level to the bottom. In (16)

$$d_{1\alpha} = -\frac{1}{2\nu_t} \left[ \frac{1}{\rho h} ((\nabla \cdot \mathbf{S})^\alpha + \tau_B^\alpha - \tau_{ss}^\alpha) - f_\alpha \right] \quad (18)$$

where  $(\nabla \cdot \mathbf{S})^\alpha$  is contravariant component of  $\nabla \cdot \mathbf{S}$ ;  $\tau_{ss}^\alpha$  represents the shear stress associated with the steady streaming and  $f_\alpha$  represents the short-wave forcing (see Putrevu and Svendsen, 1995 for detail).

$$e_{1\alpha} = \frac{\tau_B^\alpha - \tau_{ss}^\alpha}{\nu_t} \quad (19)$$

$$f_{1\alpha} + f_{2\alpha} = -\frac{Q_w^\alpha}{h} - \frac{h(\tau_B^\alpha - \tau_{ss}^\alpha)}{2\rho\nu_t} - \frac{1}{3}d_{1\alpha}h^2 \quad (20)$$

Substituting (16) into the integration forms of the coefficients  $A$ ,  $B$ ,  $D$  and  $M$  in PS99, we can get values of those dispersive mixing coefficients.

## 2.4 Boundary conditions

The boundary conditions implemented in the curvilinear version include wall boundary condition, specified-flux boundary condition, specified surface elevation boundary condition, periodic boundary condition, and moving shoreline boundary condition.

### 2.4.1 Wall boundary

Slip boundary conditions can be used for lateral walls, shorelines and boundaries of structures inside a computational domain. The contravariant technique can simplify the expressions of slip boundary conditions in curvilinear coordinates. For a curvilinear boundary, the slip boundary condition can be simply expressed as

$$\tilde{V}^\alpha = 0. \quad (21)$$

### 2.4.2 Flux boundary

A specified-flux boundary condition is implemented by using the contravariant component. The contravariant component of the specified velocity (or flux) can be obtained using the transformation relation (4).

### 2.4.3 Surface elevation boundary

Specified surface elevation boundary conditions are usually used for given tidal elevations at SHORECIRC boundaries or for model nesting between different scale circulation models.

#### 2.4.4 Periodic boundary

A periodic boundary condition along cross-shore boundaries at the two ends of the domain is also an option in this model for simulations of uniform beaches. The implementation of the periodic boundary condition is similar to that in the Cartesian version of the SHORECIRC model except that all vector variables are taken in contravariant forms. The periodic boundary condition requires both the bathymetry and grid to be periodic.

#### 2.4.5 Moving boundary

A moving boundary condition is implemented using a combined wet-dry method. The velocity of at the moving boundary is obtained by a modified Riemann solver and the shoreline is defined as an interface between dry and wet fixed grid points. The moving boundary algorithm is used in the whole computation domain including shoreline boundaries and inner structure boundaries.

## 3 Numerical Scheme

The Curvilinear SHORECIRC provides two options based on, respectively, the high-order explicit numerical schemes, as the same as in SHORECIRC, and the second-order semi-implicit schemes.

### 3.1 Staggered grid

A staggered grid in  $\xi_1 - \xi_2$  plane is employed as shown in Fig. 1, where the crosses denote  $\bar{\zeta}$ -points at which  $\bar{\zeta}$  is computed, the circles denote  $\tilde{V}^1$ -points at which  $\tilde{V}^1$  is computed and the squares denote  $\tilde{V}^2$ -points at which  $\tilde{V}^2$  is computed.

Various point types are defined in the model code to recognize different boundary conditions, which allows the model to be used in complicated domains such as harbors and tidal inlets. The point-type specification can be done by either using the grid generation program **CoastGrid** or specifying negative water depths at land points.

### 3.2 High-order numerical scheme

The high-order explicit schemes follow the Cartesian version of SHORECIRC (Svendsen *et al.*, 2000). The first-order spatial derivative terms are discretized to fourth-order accuracy using five-point finite-differencing. For example,  $f_{\xi_1}$  may be discretized at point  $j$  as

$$f_{\xi_1} = (f_{j-2} - 27f_{j-1} + 27f_j - f_{j+1})/(24\Delta\xi_1) + O(\delta\xi_1^4) \quad (22)$$

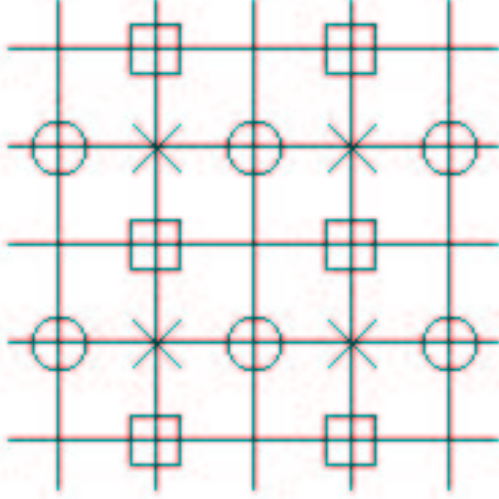


Figure 1: Staggered grid in  $\xi_1 - \xi_2$  plane ( $\times$  —  $\bar{\zeta}$  point,  $\circ$  —  $\tilde{V}^1$  and  $\square$  —  $\tilde{V}^2$ ).

The fourth-order Adams-Bashforth-Moulton predictor-corrector scheme is employed to perform time updating. A sequence of time instants are defined by  $t = p\Delta t$ . Level  $p$  refers to information at the present, known time level. For the time-derivative equation written by

$$\frac{\partial f}{\partial t} = E \quad (23)$$

the predictor step is the third-order explicit Adams-Bashforth scheme, given by

$$f_{i,j}^{p+1} = f_{i,j}^p + \frac{\Delta t}{12}[23(E)_{i,j}^p - 16(E)_{i,j}^{p-1} + 5(E)_{i,j}^{p-2}] \quad (24)$$

After predictor step we use the fourth-order Adams-Moulton corrector method:

$$f_{i,j}^{p+1} = f_{i,j}^p + \frac{\Delta t}{24}[9(E)_{i,j}^{p+1} + 19(E)_{i,j}^p - 5(E)_{i,j}^{p-1} + (E)_{i,j}^{p-2}] \quad (25)$$

### 3.3 Second-order semi-implicit scheme

As an alternative option, the second-order semi-implicit numerical schemes can be used for long-term simulations. The second-order semi-implicit numerical schemes are developed based on a splitting method in which the gravity wave mode and vorticity wave mode are solved separately. The gravity model is basically presented in the form of the ordinary nonlinear shallow water equations as

$$\frac{\delta}{\delta t}(\tilde{V}^\alpha h) + \frac{1}{\sqrt{g_0}} \frac{\partial}{\partial \xi_\beta} [\sqrt{g_0}(\tilde{V}^\alpha \tilde{V}^\beta h)] + \tilde{V}^\gamma \tilde{V}^\beta h \Gamma_{\gamma\beta}^\alpha + gh g^{\beta\alpha} \frac{\partial \bar{\zeta}}{\partial \xi_\beta} + \frac{\tau_B^\alpha}{\rho} = 0 \quad (26)$$

The vorticity mode includes the lateral mixing and the 3D dispersion effects. Radiation stresses are also calculated in the vorticity mode:

$$\begin{aligned}
\frac{\delta}{\delta t}(\tilde{V}^\alpha h) &+ \frac{1}{\sqrt{g_0}} \frac{\partial}{\partial \xi_\beta} [\sqrt{g_0}(A_{\alpha\beta\delta}\tilde{V}^\delta)] + A_{\gamma\beta\delta}\tilde{V}^\delta \Gamma_{\gamma\beta}^\alpha \\
&+ \frac{1}{\rho\sqrt{g_0}} \frac{\partial}{\partial \xi_\beta} [\sqrt{g_0}(S^{\alpha\beta} + \rho M_{\alpha\beta})] + \frac{1}{\rho}(S^{\gamma\beta} + \rho M_{\gamma\beta})\Gamma_{\gamma\beta}^\alpha \\
&+ \frac{1}{\sqrt{g_0}} \frac{\partial}{\partial \xi_\beta} \left\{ \sqrt{g_0} [T^{\alpha\beta} - h(D_{\delta\beta}\tilde{V}_{,\delta}^\alpha + D_{\delta\alpha}\tilde{V}_{,\delta}^\beta)] \right\} \\
&+ [T^{\gamma\beta} - h(D_{\delta\beta}\tilde{V}_{,\delta}^\gamma + D_{\delta\gamma}\tilde{V}_{,\delta}^\beta)] \Gamma_{\gamma\beta}^\alpha \\
&- \frac{1}{\sqrt{g_0}} \frac{\partial}{\partial \xi_\beta} [\sqrt{g_0}(hB_{\alpha\beta}\tilde{V}_{,\delta}^\delta)] - (hB_{\gamma\beta}\tilde{V}_{,\delta}^\delta)\Gamma_{\gamma\beta}^\alpha = 0
\end{aligned} \tag{27}$$

The gravity mode will be solved semi-implicitly using the regular alternative-direction-implicit method which is verified to be a CFL-free method for linearized equations (Casulli and Zanolli, 2002). Substituting the discretized Eq. (26) into Eq. (6) leads to the surface elevation alone equation:

$$-\frac{Ea(i)}{J\Delta\xi_1^2 R} \bar{\zeta}_{i-1} + \bar{\zeta}_i - \frac{Ea(i+1)}{J\Delta\xi_1^2 R} \bar{\zeta}_{i+1} = \frac{1}{R} \left( -\frac{1}{J} \frac{Eb(i+1) - Eb(i)}{\Delta\xi_1} - \frac{1}{J} \frac{\partial \tilde{v}}{\partial \xi_2} + \frac{2}{\Delta t} \bar{\zeta}_i^{dt} \right) \tag{28}$$

where  $Ea$ ,  $Eb$  and  $R$  are coefficients from the derivation. Eq. (28) can be solved fully implicitly and  $\tilde{V}^\alpha$  can be calculated directly from the following formulation:

$$\tilde{V}^\alpha = -Ea \frac{\partial \bar{\zeta}}{\partial \xi_{alpha}} + Eb \tag{29}$$

The vorticity mode is solved using explicit schemes.

## 4 Model Structure and Program

### 4.1 Flowchart

The Curvilinear SHORECIRC is one of nearshore circulation modules optionally used in the Nearshore Community Model. The Nearshore Community Model includes three calculation modules, i.e., a wave module, a nearshore circulation module and a sediment transport module. A “Master Program” is used, as an interface, to link the three modules and to handle module coupling control, internal data transfer, interpolation/extrapolation between different grid systems, and data input and output. It is recommended that users should read the Documentation and Users Manual of the Master Program to know the entire model structure and model setup.

The structure of the CURVILINEAR SHORECIRC part of the program is given in Figure 2. “Input data adapter” is used for loading wave and bathymetry information from the Mater Program while “output data adapter” for passing SHORECIRC results to the Master Program.

## 4.2 Subroutines

The following is a list of the subroutines called from CircModule. Notice that  $\xi$  and  $\eta$  here represent the coordinates  $\xi_1$  and  $\xi_2$ , respectively.

- **adapter\_circ\_to\_wave:**

pass SHORECIRC results of  $(u, v)$  and  $\eta$  to the Master Program.

- **adapter\_wave\_to\_circ:**

pass wave information to SHORECIRC.

- **boundary:**

calculation of boundary values of  $E, F$  and  $G$ .

- **bottom\_friction:**

calculation of bottom friction.

- **calculate\_E:**

calculation of  $E$  in the continuity equation.

- **calculate\_F:**

calculation of  $F$  in the momentum equation ( $\xi_1$ ).

- **calculate\_fric\_xy:**

calculation of bottom friction. Called by **bottom\_friction**.

- **calculate\_G:**

calculation of  $G$  in the momentum equation ( $\xi_2$ ).

- **calculate\_Q1\_zvc:**

calculation of flux value  $Q1$  at z-, v- and c- points.

- **calculate\_Q2\_zuc:**

calculation of flux value  $Q2$  at z-, u- and c- points.

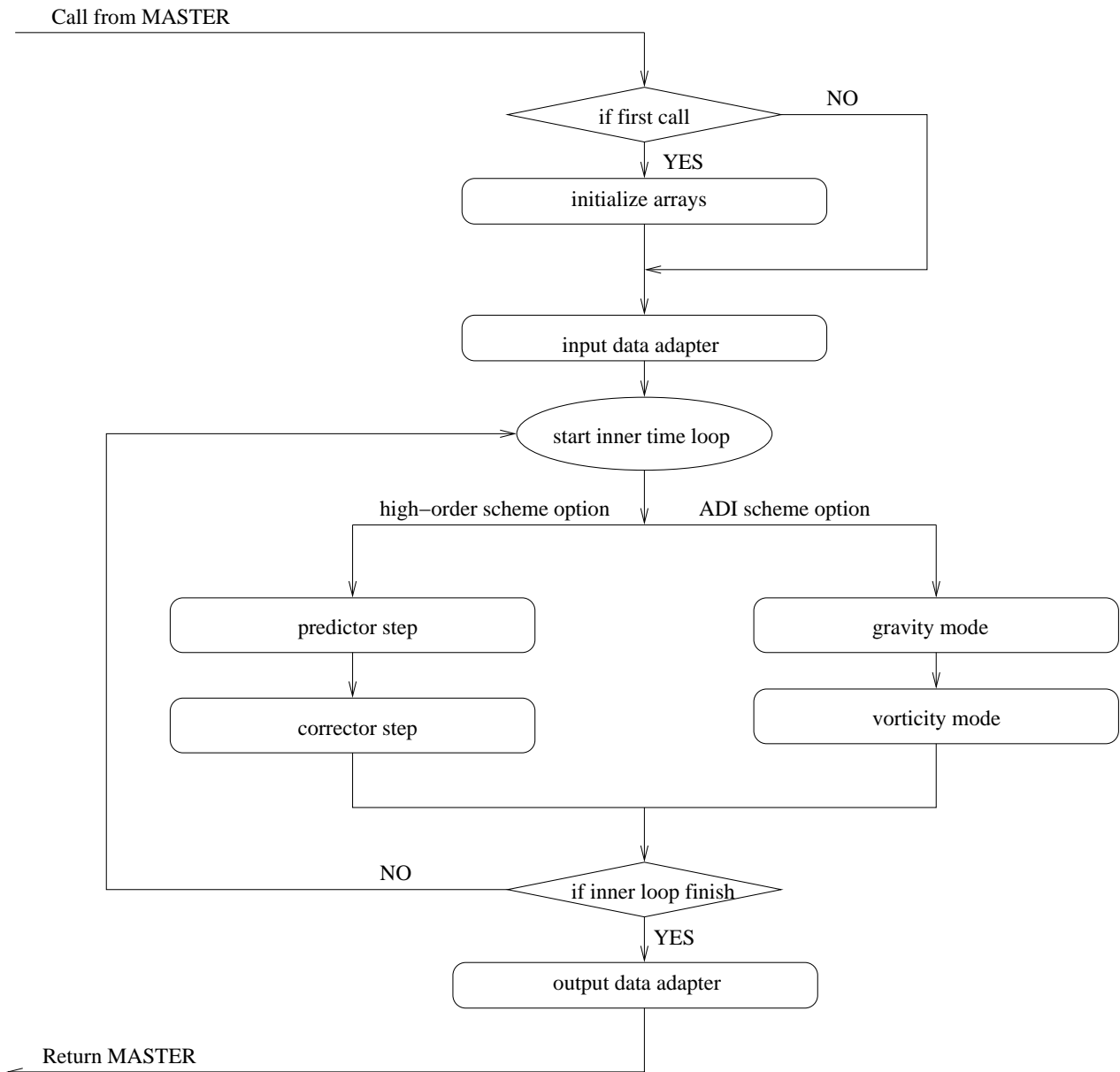


Figure 2: Flowchart of CURVILINEAR SHORECIRC

- **calculate\_QxQy:**

calculation of Cartesian flux components ( $Q_x, Q_y$ ) from contravariant components ( $Q_1, Q_2$ ).

- **calculate\_Sxx\_Sxy\_Syy\_Qw:**

calculation of Cartesian components  $S_{xx}, S_{xy}, S_{yy}$  and  $Q_w$  based on the linear wave theory when  $S_{xx}, S_{xy}, S_{yy}$  and  $Q_w$  are passed from the Master Program.

- **calculate\_u0:**

calculation of wave bottom velocity.

- **calculate\_zeta\_uvc:**

calculation of surface elevation value  $\zeta$  at u-, v- and c- points.

- **conservation:**

check on mass conservation.

- **convert\_fric\_xy:**

convert Cartesian components of bottom friction into contravariant components. Called by **bottom\_friction**.

- **convert\_Sxx\_Sxy\_Syy\_Qw:**

convert Cartesian components  $S_{xx}, S_{xy}, S_{yy}$  and  $Q_w$  to contravariant components.

- **convertUVZ:**

convert implicit-scheme based  $U, V$  and  $Z$  to hight-order-scheme based  $U, V$  and  $Z$ .

- **correct\_time\_diff:**

time discretization in corrector step, called by **correct\_stage**.

- **correct\_stage:**

corrector step.

- **curv\_C:**

calculation of curvilinear term C.

- **curv\_D:**

calculation of curvilinear term D.

- **init\_shorecirc:**

initialization of arrays in CURVILINEAR SHORECIRC.

- **depth\_u\_v:**

interpolation of depth into u- and v- points.

- **der\_eta\_at\_c\_anti\_symmetry:**

calculation of  $\frac{\partial}{\partial \eta}$  at c-point, anti-symmetric boundary condition.

- **der\_eta\_at\_c\_symmetry:**

calculation of  $\frac{\partial}{\partial \eta}$  at c-point, symmetric boundary condition.

- **der\_eta\_at\_v\_periodic\_high:**

calculation of  $\frac{\partial}{\partial \eta}$  at v-point, 4th-order scheme, periodic boundary condition.

- **der\_eta\_at\_z\_anti\_symmetry\_high:**

calculation of  $\frac{\partial}{\partial \eta}$  at z-point, 4th-order scheme, anti-symmetric boundary condition.

- **der\_u\_eta\_anti\_symmetry\_high:**

calculation of  $\frac{\partial u}{\partial \eta}$  at u-point, 4th-order scheme, anti-symmetric boundary condition.

- **der\_eta\_at\_u:**

calculation of  $\frac{\partial}{\partial \eta}$  at u-point, 2nd-order scheme.

- **der\_eta\_at\_u\_anti\_symmetry:**

calculation of  $\frac{\partial}{\partial \eta}$  at u-point, 2nd-order scheme, anti-symmetric boundary condition.

- **der\_eta\_at\_u\_symmetry:**

calculation of  $\frac{\partial}{\partial \eta}$  at u-point, 2th-order scheme, symmetric boundary condition.

- **der\_eta\_at\_u\_symmetry\_high:**

calculation of  $\frac{\partial}{\partial \eta}$  at u-point, 4th-order scheme, symmetric boundary condition.

- **der\_eta\_at\_v\_anti\_symmetry:**

calculation of  $\frac{\partial}{\partial \eta}$  at v-point, 2nd-order scheme, anti-symmetric boundary condition.

- **der\_eta\_at\_v\_symmetry:**

calculation of  $\frac{\partial}{\partial \eta}$  at v-point, 2nd-order scheme, symmetric boundary condition.

- **der\_eta\_at\_z:**

calculation of  $\frac{\partial}{\partial \eta}$  at z-point, 2nd-order scheme.

- **der\_u\_xi\_symmetry\_high:**

calculation of  $\frac{\partial u}{\partial \xi}$  at u-point, 4th-order scheme, symmetric boundary condition.

- **der\_v\_eta\_periodic:**

calculation of  $\frac{\partial v}{\partial \eta}$  at v-point, 2nd-order scheme, periodic boundary condition.

- **der\_eta\_at\_v\_symmetry\_high:**

calculation of  $\frac{\partial}{\partial \eta}$  at v-point, 4th-order scheme, symmetric boundary condition.

- **der\_eta\_at\_z\_periodic:**

calculation of  $\frac{\partial}{\partial \eta}$  at z-point, 2nd-order scheme, periodic boundary condition.

- **der\_eta\_at\_z\_specify:**

calculation of  $\frac{\partial}{\partial \eta}$  at z-point, 2nd-order scheme, specified-flux boundary condition.

- **der\_u\_xi\_periodic:**

calculation of  $\frac{\partial u}{\partial \xi}$  at u-point, 2nd-order scheme, periodic boundary condition.

- **der\_u\_xi\_specify:**

calculation of  $\frac{\partial u}{\partial \xi}$  at u-point, 2nd-order scheme, specified-flux boundary condition.

- **der\_v\_eta\_specify:**

calculation of  $\frac{\partial v}{\partial \eta}$  at v-point, 2nd-order scheme, specified-flux boundary condition.

- **der\_v\_eta\_symmetry\_high:**

calculation of  $\frac{\partial v}{\partial \eta}$  at v-point, 4th-order scheme, symmetric boundary condition.

- **der\_v\_xi\_anti\_symmetry\_high:**

calculation of  $\frac{\partial v}{\partial \xi}$  at v-point, 4th-order scheme, anti-symmetric boundary condition.

- **der\_xi\_at\_c\_anti\_symmetry:**

calculation of  $\frac{\partial}{\partial \xi}$  at c-point, 2nd-order scheme, anti-symmetric boundary condition.

- **der\_xi\_at\_c\_symmetry:**

calculation of  $\frac{\partial}{\partial \xi}$  at c-point, 2nd-order scheme, symmetric boundary condition.

- **der\_xi\_at\_u\_anti\_symmetry:**

calculation of  $\frac{\partial}{\partial \xi}$  at u-point, 2nd-order scheme, anti-symmetric boundary condition.

- **der\_xi\_at\_u\_periodic\_high:**

calculation of  $\frac{\partial}{\partial \xi}$  at u-point, 4th-order scheme, periodic boundary condition.

- **der\_xi\_at\_u\_symmetry:**

calculation of  $\frac{\partial}{\partial \xi}$  at u-point, 2nd-order scheme, symmetric boundary condition.

- **der\_xi\_at\_u\_symmetry\_high:**

calculation of  $\frac{\partial}{\partial \xi}$  at u-point, 4th-order scheme, symmetric boundary condition.

- **der\_xi\_at\_v:**

calculation of  $\frac{\partial}{\partial \xi}$  at v-point, 2nd-order scheme.

- **der\_xi\_at\_v\_symmetry:**

calculation of  $\frac{\partial}{\partial \xi}$  at v-point, 2nd-order scheme, symmetric boundary condition.

- **der\_xi\_at\_v\_symmetry\_high:**

calculation of  $\frac{\partial}{\partial \xi}$  at v-point, 4th-order scheme, symmetric boundary condition.

- **der\_xi\_at\_v\_anti\_symmetry:**

calculation of  $\frac{\partial}{\partial \xi}$  at v-point, 2nd-order scheme, anti-symmetric boundary condition.

- **der\_xi\_at\_z:**

calculation of  $\frac{\partial}{\partial \xi}$  at z-point, 2nd-order scheme.

- **der\_xi\_at\_z\_anti\_symmetry\_high:**

calculation of  $\frac{\partial}{\partial \xi}$  at z-point, 4th-order scheme, anti-symmetric boundary condition.

- **der\_xi\_at\_z\_periodic:**

calculation of  $\frac{\partial}{\partial \xi}$  at z-point, 2nd-order scheme, periodic boundary condition.

- **der\_xi\_at\_z\_specify:**

calculation of  $\frac{\partial}{\partial \xi}$  at z-point, 2nd-order scheme, specified-flux boundary condition.

- **dispersion:**

calculation of 3D dispersion terms.

- **dispersion\_coef:**  
calculation of 3D dispersion coefficients.
- **eddy\_viscosity:**  
calculation of eddy viscosity.
- **fric\_without\_u0:**  
calculation of bottom friction without effect of wave bottom velocity.
- **get\_gxx\_Cf:**  
calculation of Jacobi and the second-kind Christoffel values.
- **interp\_from\_u\_to\_c:**  
interpolation from u-points to c-points.
- **interp\_from\_v\_to\_c:**  
interpolation from v-points to c-points.
- **interp\_from\_z\_to\_c:**  
interpolation from z-points to c-points.
- **openb:**  
open boundary conditions.
- **periodic\_boundary:**  
periodic boundary conditions.
- **predict\_stage:**  
predictor step.
- **predict\_time\_diff:**  
time discretization in predictor step. Called by **predict\_stage**.
- **radiation\_stress:**  
calculation of gradient of radiation stresses.
- **shortwave\_forcing:**  
calculation of short wave forcing.

- **solve\_zeta\_u:**

solve implicit scheme-based surface elevation equation in u-direction.

- **solve\_zeta\_v:**

solve implicit scheme-based surface elevation equation in v-direction.

- **specified\_boundary:**

specified flux boundary conditions.

- **spline:**

Spline function 1 for short wave forcing transition.

- **SPLINT:**

Spline function 2 for short wave forcing transition.

- **steady\_streaming:**

calculation of steady-streaming.

- **subgrid\_diffusion:**

calcultion of subgrid diffusion.

- **subgrid\_mixing:**

calculation of subgrid mixing coefficients.

- **trig:**

tridiagonal solver

- **trig\_periodic:**

tridiagonal solver for periodic boundary condition

- **velocity:**

convert velocity values from the implicit scheme-based velocity values.

- **wind\_forcing:**

calculation of wind forcing.

## 4.3 Model input

1. **depth and grid** The information about bathymetry and computational grid is included in the input file of the Master Program *minput.f*

The following example shows the SHORECIRC-related input in *minput.f*.

&F\_NAMES

F\_depth = 'depth37x181.dat', — depth file for Master Program

F\_xycirc = ' ', — grid file for SHORECIRC, black represents the SHORECIRC grid  
is the same as the Master grid.

F\_NAME14 = 'cu.out', — output file for depth-averaged current velocity U

F\_NAME15 = 'cv.out', — output file for depth-averaged current velocity V

F\_NAME16 = 'ceta.out' — output file for surface elevation

&GRIDIN

Nx\_Circ = 37, — dimension in  $\xi_1$  direction

Ny\_Circ = 181, — dimension in  $\xi_2$  direction

Grid\_Mast\_Circ\_Same = .true., — Mast\_Grid and Circ\_Grid are same

Circ\_Staggered = .true., — staggered grid system

Circ\_Stag\_huv = 0 0 0, — Arakawa type

Circ\_Structured = .true., — structured grid

&INTERACTION

Wave\_Curr\_Interact = .true., — consider wave-current interaction

Curr\_Bed\_Interact = .true., — consider current-morphology interaction

&PASSVARIABLES

Wave\_To\_Circ\_Height = .true., — pass wave height

Wave\_To\_Circ\_Angle = .true., — pass wave angle

Wave\_To\_Circ\_WaveNum = .true., — pass wave number

Wave\_To\_Circ\_C = .true., — pass wave phase velocity

Wave\_To\_Circ\_Radiation = .true., — pass radiation stresses

Wave\_To\_Circ\_Rad\_Surf = .false., — pass surface part of radiation stresses

Wave\_To\_Circ\_Rad\_Body = .false., — pass body part of radiation stresses

Wave\_To\_Circ\_Forceing = .false., — pass short-wave forcing  
 Wave\_To\_Circ\_MassFlux = .true., — pass short-wave mass flux  
 Wave\_To\_Circ\_Dissipation = .true., — pass wave dissipation  
 Wave\_To\_Circ\_BottomUV = .true., — pass wave bottom velocity  
 Wave\_To\_Circ\_Brkindex = .true., — pass wave breaking index, “1” represents breaking  
 Circ\_To\_Wave\_UV = .true., — pass depth-averaged current velocity to wave module  
 Circ\_To\_Wave\_eta = .true., — pass time-averaged surface elevation to wave module  
 Circ\_To\_Sedi\_UV = .true., — pass depth-averaged current velocity to sediment module  
 Circ\_To\_Sedi\_UVb = .true., — pass current velocity at bottom to sediment module  
 Circ\_To\_Sedi\_eta = .true., — pass time-averaged surface elevation to sediment module  
 Circ\_To\_Sedi\_UV3D = .false., — pass 3D current velocity to sediment module  
 Circ\_To\_Sedi\_fw = .true., — pass bottom shear stress to sediment module  
 Circ\_To\_Sedi\_UVquasi3D = .false., — pass quasi-3D velocity parameter to sediment module  
 Sedi\_To\_Circ\_Depth = .true., — pass depth from sediment module to circulation module  
**&VECTORROTATE**  
 Circ\_Rotate\_Angle = 0., — coordinate system rotation angle  
**&TIMEIN**  
 N\_Interval\_CallCirc = 1, — time step interval to call circulation module

The detailed description can be found in the Master Program Users Manual.

2. **Input file for CURVILINEAR SHORECIRC** The input file named *curvcircinput.dat* is used specifically for CURVILINEAR SHORECIRC. The following is an example and brief descriptions.

**&FNAMES**

Circ\_type = ‘ ’, — boundary type file, blank means that the boundary types will be specified automatically by the model.

Circ\_specify\_flux = ' ', — input file for specified flux, blank means no flux input.  
Circ\_mask = 'mask37x181.dat', — input file for MASK. "0" for land points which will not be calculated.

/

## &NUMERICS

CR = 10, — CFL number, CR<1 for high-order schemes, 0<CR<100 for ADI schemes.

curv\_grid=0, — "0" for rectangular grid and "1" for curvilinear grid.

orth\_grid=1, — "1" for orthogonal grid and "0" for non-orthogonal grid.

plotintra=1000., — time interval (second) for SHORECIRC-only output

/

## &BOUNDARY

east\_ele2\_flx3\_grd4\_rad5\_per6=1,

— EAST boundary conditions: "1" - wall; "2" - elevation; "3" - flux; "4" - gradient; "5" - radiation; "6" - periodic.

jstart\_E=1, — starting grid point for EAST boundary

jend\_E=100, — ending grid point for EAST boundary

east\_data1\_anly2=2, — boundary data input, "1" - data; "2" - analytical

west\_ele2\_flx3\_grd4\_rad5\_per6=3,

— WEST boundary conditions: "1" - wall; "2" - elevation; "3" - flux; "4" - gradient; "5" - radiation; "6" - periodic.

jstart\_W=1, — starting grid point for WEST boundary

jend\_W=200, — ending grid point for WEST boundary

west\_data1\_anly2=2, — boundary data input, "1" - data; "2" - analytical

south\_ele2\_flx3\_grd4\_rad5\_per6=3,

— SOUTH boundary conditions: "1" - wall; "2" - elevation; "3" - flux; "4" - gradient; "5" - radiation; "6" - periodic.

istart\_S=1, — starting grid point for SOUTH boundary

iend\_S=100, — ending grid point for SOUTH boundary

south\_data1\_anly2=2, — boundary data input, "1" - data; "2" - analytical

```

north_ele2_flg3_grd4_rad5_per6=3,
    — NORTH boundary conditions: “1” - wall; “2” - elevation; “3” - flux; “4” -
    gradient; “5” - radiation; “6” - periodic.

istart_N=1, — starting grid point for NORTH boundary
iend_N=100, — ending grid point for NORTH boundary
north_data1_anly2=2, — boundary data input, “1” - data; “2” - analytical
/
&PHYSICS
f_cwc = 0, — bottom friction parameter
rmanning = 0.017, — parameter used in the Manning formula
hi=0.15, — minimum depth used in flooding calculation
delta = 0.00001, —  $\delta\eta$  in the wet-dry criterion
c_subgrid = 0.15, — subgrid mixing coefficient
anu_tb_const=0.0001, — constant background eddy viscosity coefficient
anu_t0_const=0.0001, — starting value in eddy viscosity calculation
disp3d = 1, — “1” for calculation of 3D dispersion term
depth_min=0.2, — minimum water depth
wind_u = 0., — u (m/s) component of wind
wind_v = 0., — v (m/s) component of wind
/

```

## 4.4 Model output

### 1. Screen output

The screen output includes output from the Master Program and all the three modules. The output only presents the executive progress and is usually useful for debugging purposes. The program sometimes writes out a warning or error messages when the model encounters a problem. The ordinary output looks like the following,

wave module initialization ...

call wave module ...

initialize circulation module ...

```
dt= 2.06896544 ntime= 145
circulation module ...
sediment module initialization ...
sediment module .....
Time = 300.s
circulation module ...
mexport routine
Time = 600.s
call wave module ...
circulation module ...
mexport routine
Time = 900.s
circulation module ...
sediment module .....
mexport routine
```

## 2. Output to files

The output to files is carried out in the Master Program. Users can read the Master Program Users Manual for details.

## 4.5 Passing variables in model coupling

### 1. variables passing from the circulation module to the Master Program

- Pass\_U — u component of depth-averaged velocity
- Pass\_V — v component of depth-averaged velocity
- Pass\_Ub — u component of bottom velocity
- Pass\_Vb — v component of bottom velocity
- Pass\_eta — time-averaged surface elevation
- Pass\_d11 —  $d_{11}$  in calculation of vertical profile of current velocity
- Pass\_d12 —  $d_{12}$  in calculation of vertical profile of current velocity
- Pass\_e11 —  $e_{11}$  in calculation of vertical profile of current velocity

- Pass\_e12 —  $e_{12}$  in calculation of vertical profile of current velocity
- Pass\_f11 —  $f_{11}$  in calculation of vertical profile of current velocity
- Pass\_f12 —  $f_{12}$  in calculation of vertical profile of current velocity
- Pass\_fw — bottom shear stress

## 2. variables passing from the Master Program to the circulation module

- Intp\_Fx\_Circ — x-component of short-wave forcing
- Intp\_Fy\_Circ — y-component of short-wave forcing
- Intp\_ubott\_Circ — wave bottom velocity
- Intp\_Theta\_Circ — wave angle
- Intp\_Height\_Circ — wave height
- Intp\_C\_Circ — wave phase velocity
- Intp\_WaveNum\_Circ — wave number
- Intp\_ibrk\_Circ — wave breaking index
- Intp\_Sxx\_Circ — radiation stress  $S_{xx}$
- Intp\_Sxy\_Circ — radiation stress  $S_{xy}$
- Intp\_Syy\_Circ — radiation stress  $S_{yy}$
- Intp\_Sxx\_Surf — surface part of radiation stress  $S_{xx}$  for 3D circulation module
- Intp\_Sxy\_Surf — surface part of radiation stress  $S_{xy}$  for 3D circulation module
- Intp\_Syy\_Surf — surface part of radiation stress  $S_{yy}$  for 3D circulation module
- Intp\_Sxx\_Body — body part of radiation stress  $S_{xx}$  for 3D circulation module
- Intp\_Sxy\_Body — body part of radiation stress  $S_{xy}$  for 3D circulation module
- Intp\_Syy\_Body — body part of radiation stress  $S_{yy}$  for 3D circulation module
- Intp\_MassFluxU\_Circ — u component of short wave mass flux
- Intp\_MassFluxV\_Circ — v component of short wave mass flux
- Intp\_Diss\_Circ — wave dissipation

## 5 Curvilinear Grid Generation

A curvilinear grid can be generated using the grid generation tool **CoastGrid**. **CoastGrid** is based on Brackbill (1982)'s adaptive grid generation method and designed for the curvilinear versions of the SHORECIRC model and Boussinesq model. The Matlab program of **CoastGrid** can be download from

<http://chinacat.coastal.udel.edu/kirby/programs/index.html>

The **CoastGrid** will generate a grid type file and a gird coordinate file which can be directly used in CURVILINEAR SHORECIRC. For more information, visit

<http://www.coastal.udel.edu/fyshi/gridmk/gridhome.html>

## 6 Test Examples

This section will show a test case of the longshore current simulation in an obliquely quadrilateral tank. We will provide more test cases with complex computational domains when measurement data available.

### 6.1 Longshore current simulation in an obliquely quadrilateral domain

This test case describes the simulation of wave-induced longshore currents on a plane beach. The corresponding laboratory experiment was carried out in the Large-scale Sediment Transport Facility (LSTF) at the U.S. Army Engineer Research and Development Center's Coastal and Hydraulics Laboratory (Hamilton and Ebersole, 2001). The LSTF has a concrete beach which has a longshore dimension of 31m and a cross-shore dimension of 21m, with a plane slope of 1 : 30. To reproduce a longshore uniform current in the finite-length wave basin, 20 independent pumps and channels are used to control the cross-shore distribution of the mean longshore current. To minimize wave diffraction into the flow channels, two obliquely oriented waveguides oriented 10 degrees from the shoreline-normal direction were set on lateral boundaries. Figure 3 shows a plan view of the LSTF and locations of waveguides and measurement transects (dashed lines). In the figure,  $Q_p$  is the total longshore flow rate actively pumped through the external recirculation system. If the wave-induced longshore current does not match  $Q_p$ , an internal recirculation  $Q_r$  will develop as shown in the figure. The  $Q_s$  is the total longshore flow rate between the wave set-up limit and the point of transition where the mean longshore current reverses direction. In the physical experiment, the discharge from the pumps was adjusted to minimize

the internal recirculation  $Q_r$ . This technique was previously used by Visser (1980, 1984 and 1991).

### 6.1.1 General model description

For this simulation, we should consider the internal recirculation and the boundary effect of oblique waveguides showing up near the lateral boundaries. A boundary-fitted grid is generated as shown in Figure 4. The grid sizes are  $0.5m$  in longshore direction and  $0.26m$  along the waveguide direction ( $0.25m$  between two adjacent longshore-direction grid lines). The grid data files for the CURVILINEAR SHORECIRC and the Master Program are *xycirc\_test1.dat* and *xymast\_test1.dat*, included in the example package.

As a specified volume flux boundary condition, the measured flux at the lateral boundaries is employed by interpolating the data into the model boundary points. The data file is *flux\_test1.dat* in the example package. The offshore boundary and shoreline boundary are vertical walls as specified in *curvcircinput.dat*.

A regular wave case was simulated from the physical experiment with a wave period of  $2.5s$ ,  $0.182m$  incident wave height and 10-degree wave angle. The water depth decreases linearly from  $0.667m$  at the offshore boundary to  $0.002m$  at the shoreline boundary. The bathymetry file is *depth\_test1.dat*. The CFL number used in this case is  $0.5$ . Wave-current interaction is taken into account in the model by calling the wave-driver subroutine every  $10s$ . The model reached steady state after  $200s$ .

### 6.1.2 Input files

1. Input file for the Master Program *minput.dat*

```
&F_NAMES
F_depth = 'depth_test1.dat',
F_xymast = 'xymast_test1.dat'
F_xywave = ' ',
F_xycirc = 'xycirc_test1.dat',
F_xysedi = ' ',
F_NAME6 = ' ',
F_NAME7 = ' ',
F_NAME8 = ' ',
F_NAME9 = ' ',
```

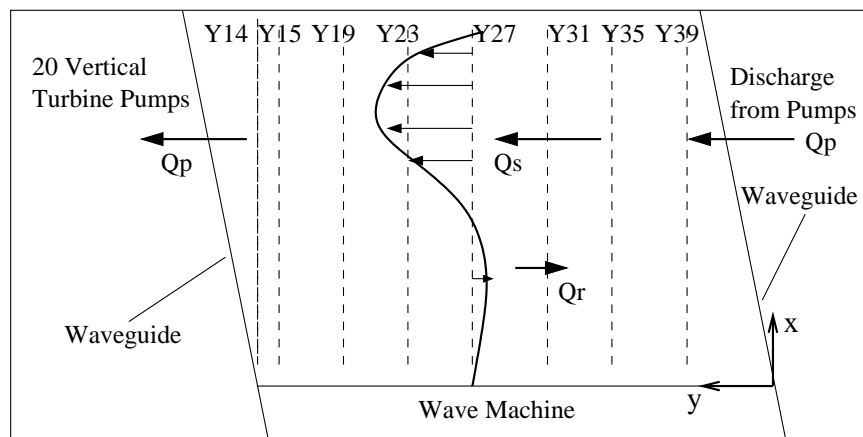


Figure 3: Plan view of the LSTF.

```

F_NAME10 = '',
F_NAME11 = '',
F_NAME12 = '',
F_NAME13 = 'wheight.out',
F_NAME14 = 'cu.out',
F_NAME15 = 'cv.out',
F_NAME16 = 'ceta.out'/
&GRIDIN
Nx_Mast = 85,
Ny_Mast = 71,
Nx_Circ = 85,
Ny_Circ = 63,
Nx_Wave = 85,
Ny_Wave = 71,
Nx_Sedi = 85,
Ny_Sedi = 71,
Grid_Mast_Wave_Same = .true.,
Grid_Mast_Circ_Same = .false.,
Grid_Mast_Sedi_Same = .true.,
Wave_Staggered = .false.,
Wave_Stag_huv = 0 0 0,
Circ_Staggered = .true.,
Circ_Stag_huv = 1 2 3,
Sedi_Staggered = .false.,
Sedi_Stag_huv = 0 0 0,
Wave_Structured = .true.,
Circ_Structured = .true.,
Sedi_Structured = .true.,
Grid_Extrapolation = .false.,

```

```
/  
 &INTERACTION  
Wave_Curr_Interact = .true.,  
Wave_Bed_Interact = .false.,  
Curr_Bed_Interact = .false.,  
  
/  
 &PASSVARIABLES  
Wave_To_Circ_Height = .true.,  
Wave_To_Circ_Angle = .true.,  
Wave_To_Circ_WaveNum = .true.,  
Wave_To_Circ_C = .true.,  
Wave_To_Circ_Radiation = .true.,  
Wave_To_Circ_Rad_Surf = .false.,  
Wave_To_Circ_Rad_Body = .false.,  
Wave_To_Circ_Forceing = .false.,  
Wave_To_Circ_MassFlux = .true.,  
Wave_To_Circ_Dissipation = .true.,  
Wave_To_Circ_BottomUV = .true.,  
Wave_To_Circ_Brkindex = .true.,  
Circ_To_Wave_UV = .true.,  
Circ_To_Wave_eta = .true.,  
Wave_To_Sedi_Height = .true.,  
Wave_To_Sedi_Angle = .true.,  
Wave_To_Sedi_BottomUV = .true.,  
Circ_To_Sedi_UV = .true.,  
Circ_To_Sedi_UVb = .true.,  
Circ_To_Sedi_eta = .true.,  
Circ_To_Sedi_UV3D = .false.,  
Circ_To_Sedi_fw = .true.,
```

```

Circ_To_Sedi_UVquasi3D = .false.,
Sedi_To_Wave_Depth = .true.,
Sedi_To_Circ_Depth =.true.,
/
&VECTORROTATE
Circ_Rotate_Angle = 0.,
Wave_Rotate_Angle = 0.,
Sedi_Rotate_Angle = 0.,
/
&TIMEIN
Total_Time = 400,
Master_dt = 10,
N_Interval_CallWave = 1,
N_Interval_CallCirc = 1,
N_Interval_CallSedi = -1,
N_Delay_CallSedi =1,
N_Interval_Output = 1,
/

```

2. Input file for the REF/DIF-1 wave module *indat.dat*

```

&FNAMES
FNAME2 = ' ',
FNAME3 = ' ',
FNAME4 = 'wave.dat',
FNAME5 = 'refdif1.log',
FNAME6 = 'height.dat',
FNAME7 = 'angle.dat',
FNAME8 = ' ',
FNAME9 = ' ',

```

```
FNAME10 = 'sxx.out',
FNAME11 = 'sxy.out',
FNAME12 = 'syx.out',
FNAME13 = '',
FNAME14 = '',
FNAME15 = '',
FNAME16 = '',
FNAME17 = '',
FNAME18 = '',
FNAME19 = '',
FNAME20 = '',
FNAME21 = '',
FNAME22 = '',
FNAME23 = '',
FNAME24 = '',
FNAME25 = '',
FNAME26 = '',
/
&INGRID
MR = 85,
NR = 71,
IU = 1,
NTYPE = 0,
ICUR = 0,
IBC = 1,
ISMOOTH = 0,
DXR = 0.25,
DYR = 0.5,
DT = 10.,
```

```

ISPACE = 0,
ND = 1,
IFF = 0 0 1,
ISP = 0,
IINPUT = 1,
IOOUTPUT = 1/
&WAVES1A
IWAVE = 1,
NFREQS = 1/
&WAVES1B
FREQS = 2.5,
TIDE = 0.,
NWAVS = 1,
AMP = 0.091,
DIR = 10./

```

3. Input file for the CURVILINEAR SHORECIRC *curvcircinput.dat*

```

&FNAMES
Circ_type = ' ',
Circ_specify_flux = 'flux_test1.dat',
Circ_mask = ' ',
/
&NUMERICS
CR = 0.5,
curv_grid=1,
orth_grid=0,
plotintra=1.,
/
&BOUNDARY

```

```

east_ele2_flx3_grd4_rad5_per6=1,
jstart_E=1,
jend_E=100,
east_data1_anly2=2
west_ele2_flx3_grd4_rad5_per6=1,
jstart_W=1,
jend_W=200,
west_data1_anly2=2
south_ele2_flx3_grd4_rad5_per6=3,
istart_S=1,
iend_S=100,
south_data1_anly2=1
north_ele2_flx3_grd4_rad5_per6=3,
istart_N=1,
iend_N=100,
north_data1_anly2=1
/
&PHYSICS
f_cwc = 0,
rmanning = 0.017
hi=0.15
delta = 0.15
c_subgrid = 1.5,
anu_tb_const=0.0001,
anu_t0_const=0.0001,
disp3d = 1,
depth_min=0.002,
wind_u = 0.,
wind_v = 0.,
/

```

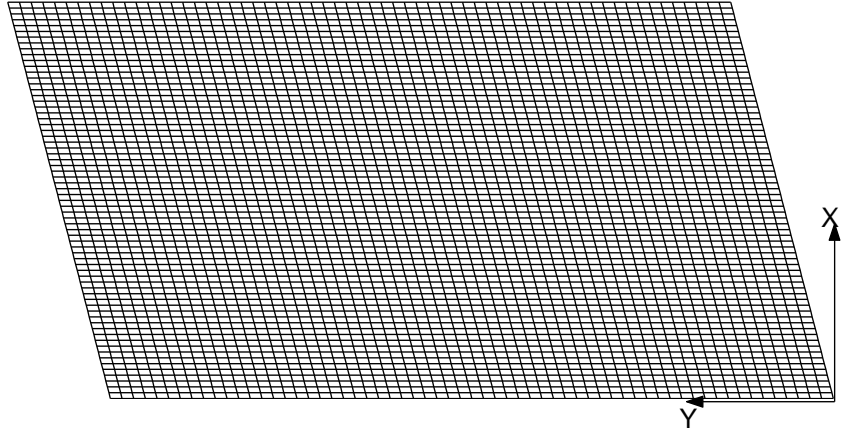


Figure 4: Computational grid.

### 6.1.3 Results

Figure 5 shows the calculated depth-averaged current field. It shows that the steady state longshore current appears approximately longshore uniform. The peak currents are around  $x = 12 - 15m$  in the surfzone while the breaking line is around  $x = 9m$  in both the physical experiment and the REF/DIF-1 results. There is a very weak internal recirculation outside the surfzone, found in the numerical results and confirmed by the experimental data.

The longshore current comparisons are made between the numerical results and experiment measurements at 8 measurement transects shown by dashed lines in Figure 3. Figure 6 shows the comparisons, where  $y = 5.7, 9.7, 13.7, 17.7, 21.7, 25.7, 29.7$  and  $30.7m$  in the figure are the model coordinates and represent the locations of the corresponding measurement transects Y39, Y35, Y31, Y27, Y23, Y19, Y15, and Y14, respectively, shown in Figure 3. As shown in Figure 6, the current amplitudes and the locations of peak currents are well predicted. Some apparent disagreements are found in the downstream transects of  $y = 29.7m$  and  $30.7m$ , where the measured current data show a different cross-shore variation around  $x = 12m$ . This particular feature is not resolved by the model predictions. Also, an under-prediction of the currents is found near the shoreline region in the same two transects. In Figure 7, we compare the measured mean water levels and the numerical results. The figure shows that very good agreement is obtained from the comparisons of wave set-up and set-down.

The LSTF measurements also provide information about the vertical variation of the currents. Figure 8 shows the model/data comparisons of cross-shore velocities at measure-

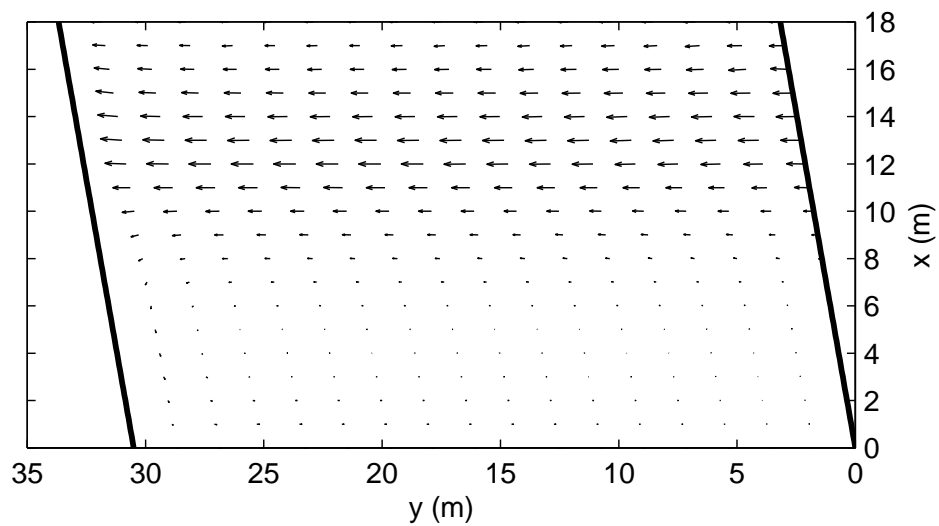


Figure 5: Depth-averaged current velocity field.

ment points in transect Y27.

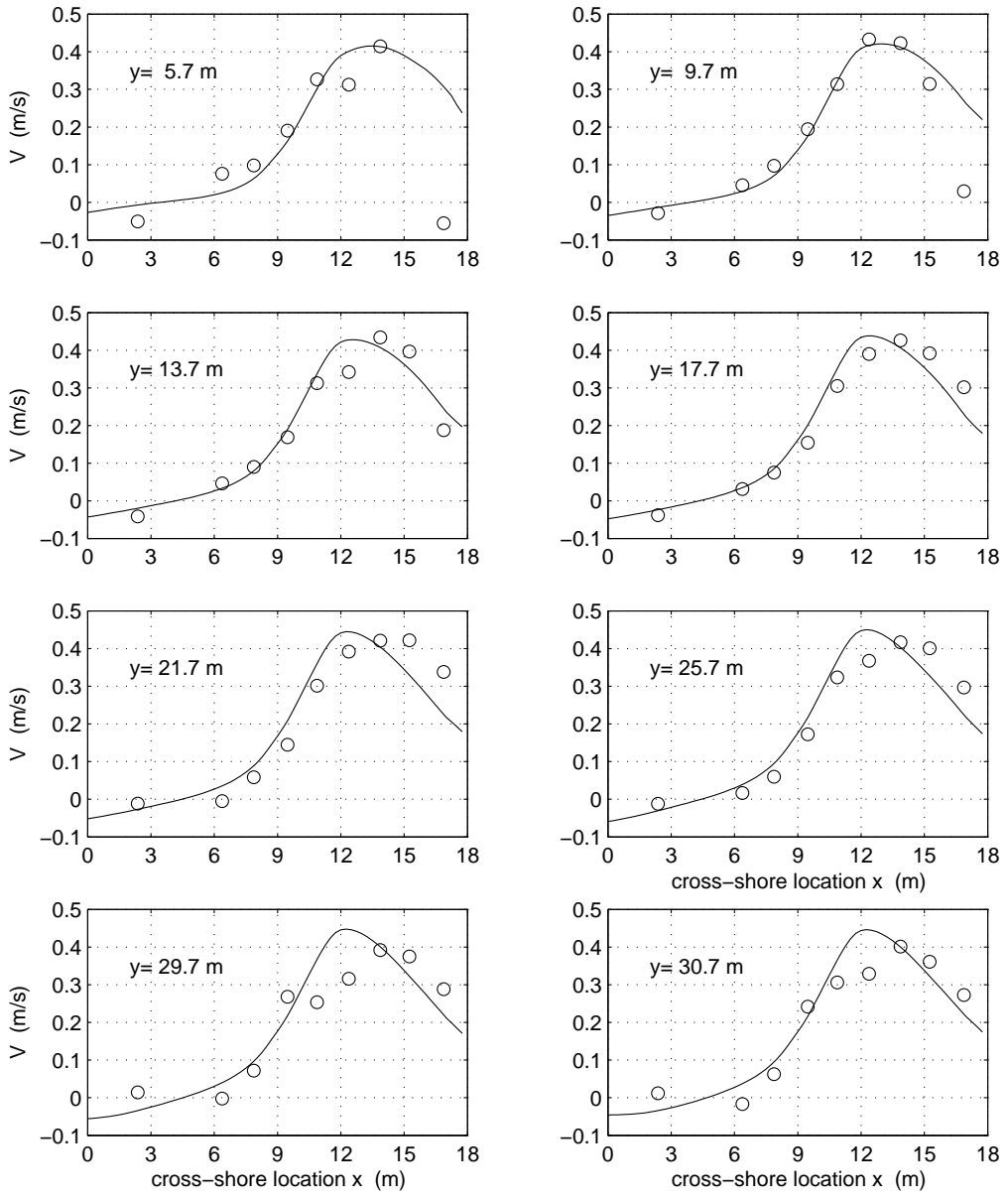


Figure 6: Longshore current comparisons at the measurement transects (circles: measurement, solid lines: numerical results).

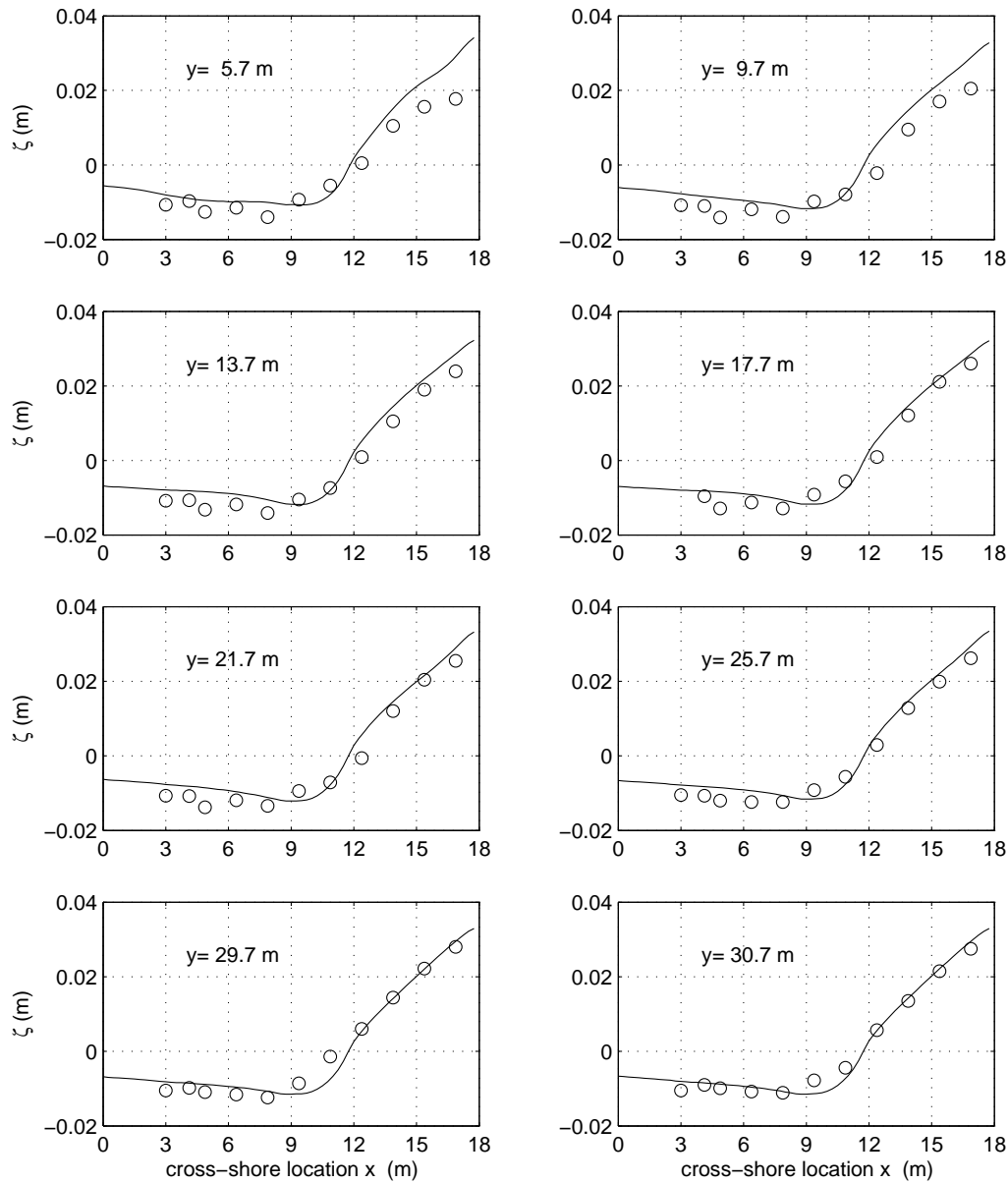


Figure 7: Mean water level comparisons at the measurement transects (circles: measurement, solid lines: numerical results).

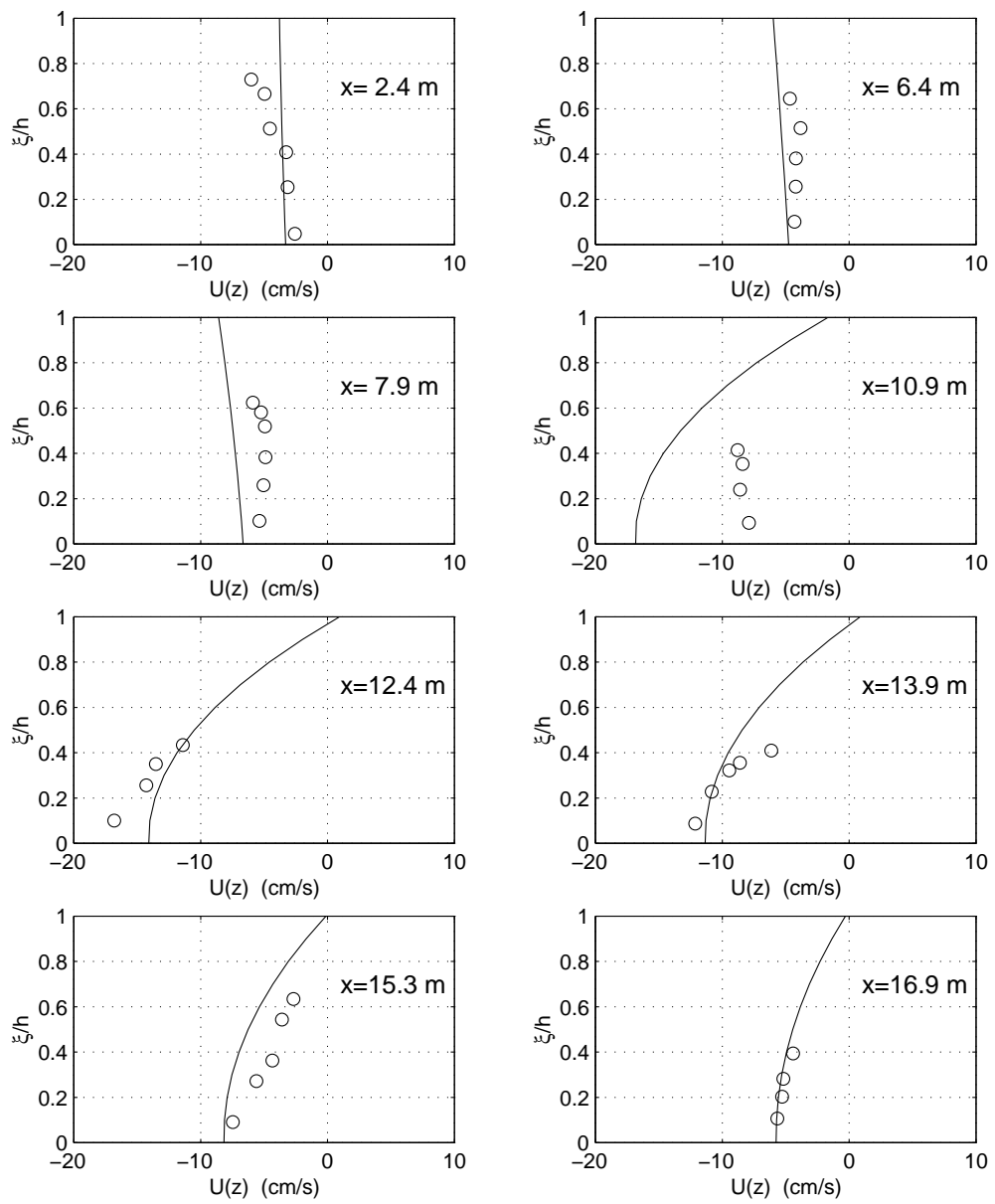


Figure 8: Comparison of the vertical profile of cross-shore current at Y27 (circles: measurement, solid lines: numerical results).

## 7 References

- Blumberg, A. F. and G. L. Mellor, A description of a three-dimensional coastal ocean circulation model, *Three-Dimensional Coastal Ocean Models*, edited by N. Heaps, pp.208, American Geophysical Union, 1987.
- Borthwick, A. G. L. and Barber, R. W., 1992, River and reservoir flow modeling using the transformed shallow water equations, *Int. J. Numer. Methods Fluids*, 14, 1193-1217.
- Brackbill, J. U. and Saltzman, J. S., 1982, Adaptive zoning for singular problems in two dimensions, *J. Comput. Phys.*, 46, 342-368.
- Brocchini M., Svendsen, I. A., Prasad, R., and Bellotti, G., 2001, A comparison of two different types of shoreline boundary conditions, *J. Comp. Meth. in Appl. Mech. and Engng.*, Vol. 191 (39-40), pp. 4575-4596.
- Casulli, V. and Zanolli, P., 2002, “Semi-implicit numerical modeling of nonhydrostatic free-surface flows for environmental problem” *Mathematical and Computer Modelling*, 36, 1131-1149.
- Hamilton, D. G. and Ebersole, B. A., 2001, Establishing uniform longshore currents in a large-scale sediment transport facility, *Coastal Engineering*, 42, 199-218.
- Haas, K., Svendsen, I. A. and Haller, M. C., 1998, Numerical modeling of nearshore circulation on a barred beach with rip channels, In *Proc. 26th Int. Conf. on Coast. Engrg.*, Copenhagen, 801-814.
- Häuser, J., Paap, H. G., Eppel, D. and Mueller, A., 1985, Solution of shallow water equations for complex flow domains via boundary fitted coordinates, *Int. J. Numer. Methods Fluids*, 5, 727-744.
- Häuser, J., Paap, H. G., Eppel, D. and Sengupta, S., 1986, Boundary conformed coordinate systems for selected two-dimensional fluid flow problems. Part 2: Application of the BFG method, *Int. J. Numer. Methods Fluids*, 6, 529-539.
- Kirby, J. T. and Dalrymple, R. A., 1986, Modeling waves in surfzones and around islands, *J. Waterway, Port, Coastal and Ocean Engineering*, 112: 78-93.
- Kirby, J. T., Dalrymple, R. A. and Shi, F., 2002, Combined Refraction/Diffraction Model REF/DIF 1, Version 2.6. Documentation and User’s Manual, Research Report No.CACR-02-02, Center for Applied Coastal Research, Department of Civil and Environmental Engineering, University of Delaware, Newark.

- Putrevu, U. and Svendsen, I. A., 1995, Vertical structure of the undertow outside the surf zone, *J. Geophys. Res.*, 98, 22, 707-22, 716.
- Putrevu, U. and Svendsen, I. A., 1999, Three-dimensional dispersion of momentum in wave-induced nearshore currents, *Eur. J. Mech. B/Fluids*, 83-101.
- Raghunath, R., Sengupta, S. and Häuser, J., 1987, A study of the motion in rotating containers using a boundary-fitted coordinate system, *Int. J. Numer. Methods Fluids*, 7, 453-464.
- Sancho, F. E., Svendsen, I. A., Van Dongeren, A. R. and Putrevu, U., 1995, Longshore nonuniformities of nearshore currents, *Coastal Dynamics'95*, Gdansk, 425-436.
- Sancho, F. E. and Svendsen, I. A., 1998, Shear waves over longshore nonuniform barred beaches, In *Proc. 26th Int. Conf. on Coast. Engrg.*, Copenhagen, 230-243.
- Sheng, Y. P., 1986, Modeling coastal and estuarine processes using boundary-fitted grids, *Proceedings 3rd Int'l Symposium on River Sedimentation*, 1416-1442.
- Shi, F. and Sun, W., 1995, A variable boundary model of storm surge flooding in generalized curvilinear coordinate grids, *Int. J. Num. Methods Fluids*, 21, 641-651.
- Shi, F., Sun, W. and Wei, G., 1997, A WDM method on generalized curvilinear grid for calculation of storm surge flooding, *Applied Ocean Research*, 19, 275-282.
- Shi, F., Dalrymple R. A., Kirby, J. T., Chen, Q. and Kennedy, A., 2001, A fully nonlinear Boussinesq model in generalized curvilinear coordinates, *Coastal Engineering*, 42, 237-258.
- Smith, R., 1997, Multi-mode models of flow and of solute dispersion in shallow water. Part 3. Horizontal dispersion tensor for the velocity, *J. Fluid Mech.*, 352, 331-340.
- Svendsen, I. A. and Putrevu, U., 1994, Nearshore mixing and dispersion, *Proc. Roy. Soc. Lond. A*, 445, 561-576.
- Svendsen, I. A., Sancho, F. E., Oltman-Shay, J. and Thornton, E. B., 1997, Modelling nearshore circulation under field conditions, *Proceedings Waves'97 Conference*, Virginia Beach, 765-776.
- Svendsen, I. A. and Haas, K., 1999, Interaction of undertow and rip currents, In *Proc. 5th Int. Conf. Coastal and Port Engrg. Developing Countries*, Cape Town, 218-229.

- Svendsen, I. A., Haas, K., and Zhao, Q., 2000, Quasi-3D nearshore circulation model, SHORECIRC, Version 1.3.6, Report, Center for Applied Coastal Research, University of Delaware, Newark.
- Taylor, G. I., 1953, Dispersion of soluble matter in solvent flowing slowly through a tube, *Proc. Roy. Soc. Lond. A*, 219, 186-203.
- Taylor, G. I., 1954, The dispersion of matter in a turbulent flow through a pipe, *Proc. Roy. Soc. Lond. A*, 219, 446-468.
- Van Dongeren, A. R., Svendsen, I. A. and Sancho, F. E., 1995, Application of the Q-3D SHORECIRC model to surfbeat, *Coastal Dynamics'95*, Gdansk, 233-244.
- Van Dongeren, A. R., Svendsen, I. A. and Sancho, F. E., 1996, Generation of infragravity waves, In *Proc., 25th Int. Conf. on Coast. Engrg.*, Orlando, 1335-1348.
- Van Dongeren, A. R. and Svendsen, I. A., 1997, An absorbing-generating boundary condition for shallow water models, *J. Waterway, Port, Coastal, and Ocean Eng.*, 123, 303-313.
- Van Dongeren, A. R., Svendsen, I. A. and Putrevu, U., 1998, Quasi 3-D effects in leaky infragravity waves, in *Proc. 26th Int. Conf. on Coast. Engrg.*, Copenhagen, 1323-1336.
- Van Dongeren, A. R. and Svendsen, I. A., 2000, Nonlinear and 3D effects in leaky infragravity waves, *Coastal Engineering*, 41, 467-496.
- Visser, P. J., 1980, Longshore current flows in a wave basin, In *Proc., 17th Int. Conf. on Coast. Engrg.*, Sydney, 462-479.
- Visser, P. J., 1984, Uniform longshore current measurements and calculations, In *Proc., 19th Int. Conf. on Coast. Engrg.*, Houston, 2192-2207.
- Visser, P. J., 1991, Laboratory measurements of uniform longshore currents, *Coastal Engineering*, 15, 563-593.
- Warsi, Z. U. A., 1998, *Fluid Dynamics: Theoretical and Computational Approaches*, 2nd ed. CRC Press, New York.
- Wei, G., Kirby, J. T., 1995, A time-dependent numerical code for the extended Boussinesq equations, *J. Waterw., Port, Coastal Ocean Eng.* 121 (5), 251-261.